Electronic Supplementary Material (ESI) for Materials Advances.


# Magnetoresponsive biocomposite hydrogels comprising of gelatin and valine based magnetic ionic liquid surfactant as controlled release nanocarrier for drug delivery

Akshay Kulshrestha,[ab] Sanjay Sharma,[c] Kuldeep Singh,[ab] and Arvind Kumar[ab]*

[a]Academy of Scientific and Innovative Research (AcSIR), Ghaziabad-201002, India.

[b]CSIR-Central Salt and Marine Chemicals Research Institute, Council of Scientific and Industrial Research, G. B. Marg, Bhavnagar, 364002, Gujarat India.

[c]Department of Chemistry, Institute of Integrated & Honors Studies, Kurukshetra University, Kurukshetra, India.

**Table of contents**

## 1. Structural scheme of synthesized $[ValC_{16}][FeCl_4]$.

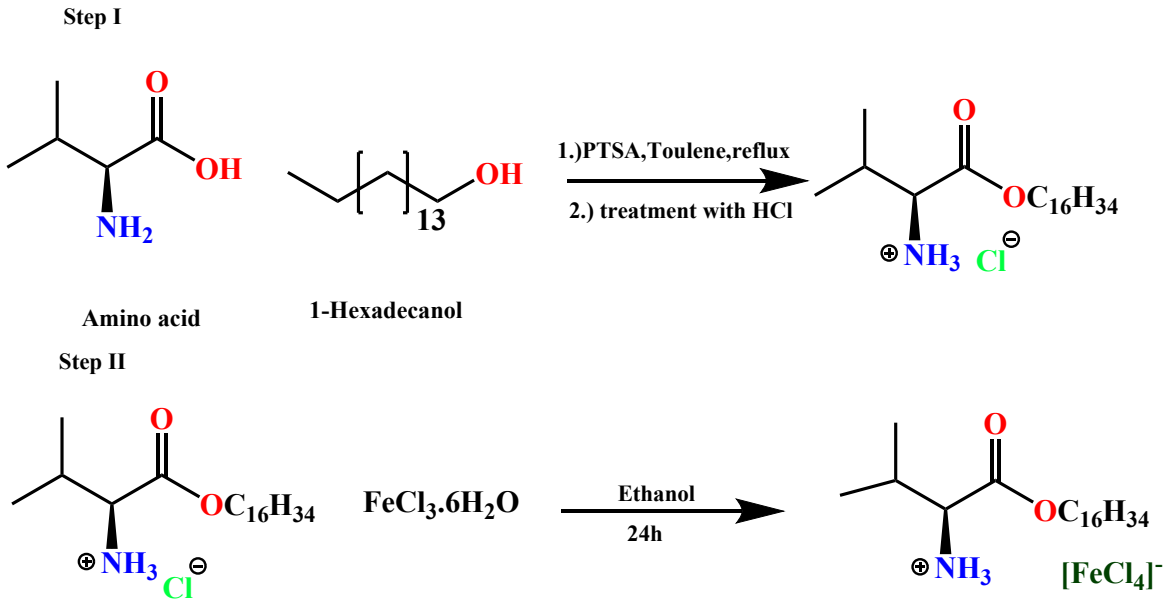


**Fig. S1.** Synthetic procedure of $[ValC_{16}][FeCl_4]$ .

## 2. $^{1}$H NMR of the synthesis of [ValC$_{16}$][FeCl$_4$]

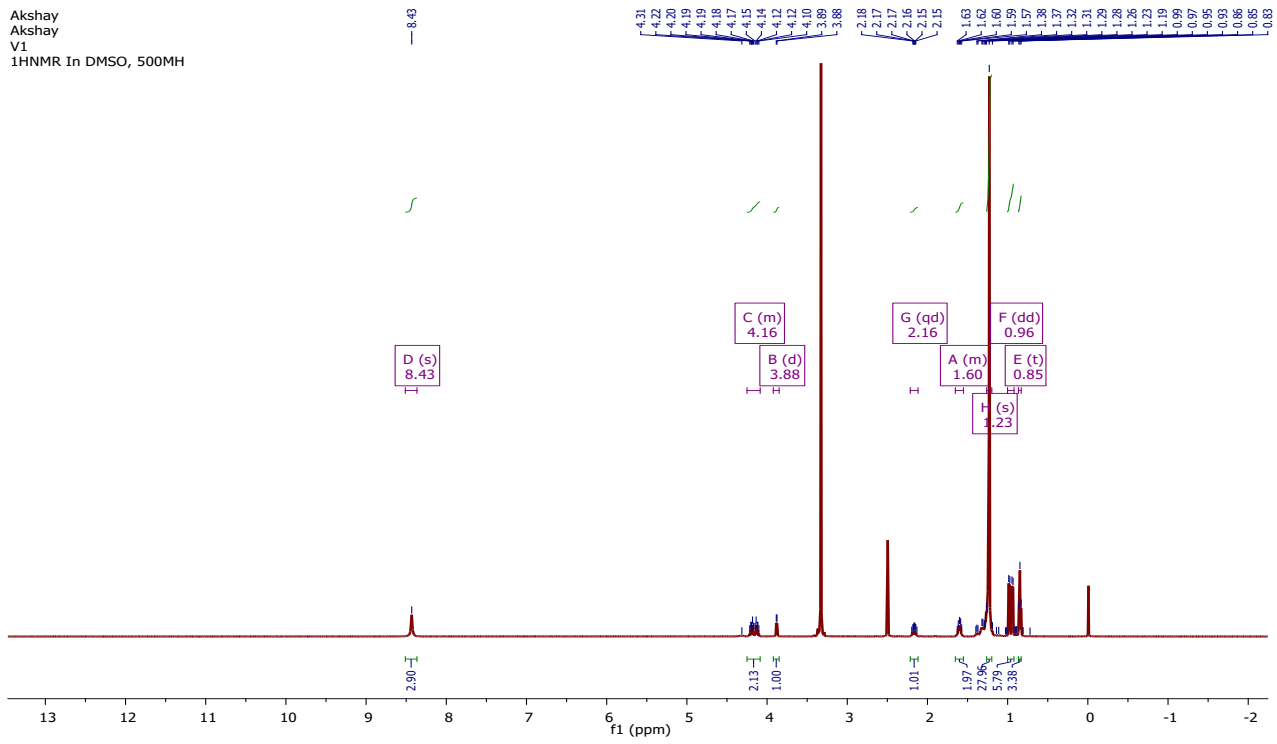


**Fig. S2:** $^{1}$H NMR of [ValC$_{16}$][Cl]

**$^{1}$H NMR chemical shift values of [ValC$_{16}$][Cl]** $CDCl_3$, 500MH$_z$: $\delta_H$ (ppm) 8.43 (s, 3H), 4.16(m, 3H), 3.98(t,2H ), 2.16(s,1H), 1.60 (m,2H), 1.25-1.29(m, 26H,$CH_2$), 0.96(dd, 6H), 0.85(t,3H**).**

## 3. LCMS of the synthesis of $[ValC_{16}][FeCl_4]$

LCMS of $[ValC_{16}][FeCl_4]$: ESI+ 342.3, ESI – 197.8

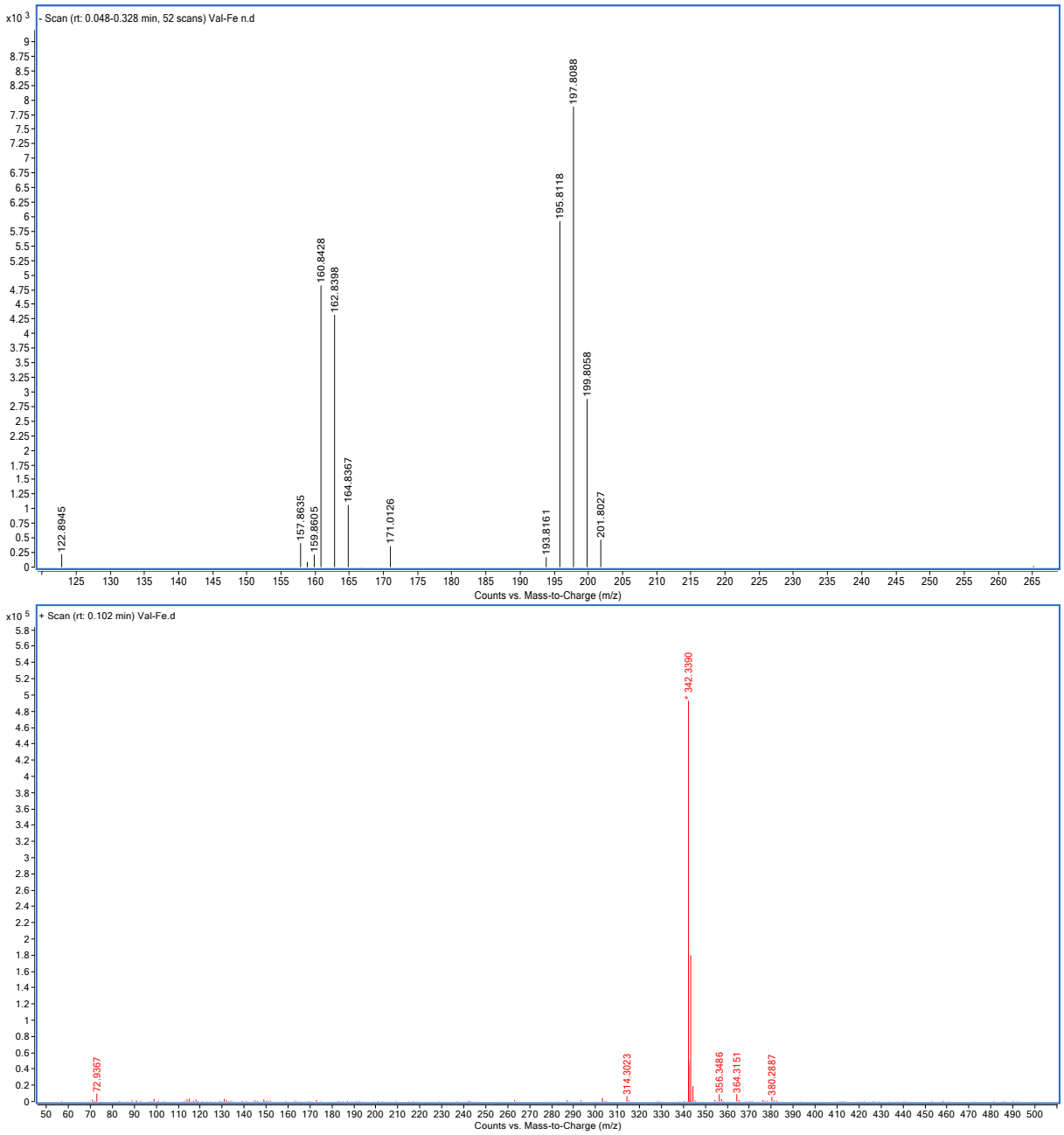


**Fig. S3** LCMS of of $[ValC_{16}][FeCl_4]$.

## 4. Raman spectra of $[ValC_{16}][FeCl_4]$

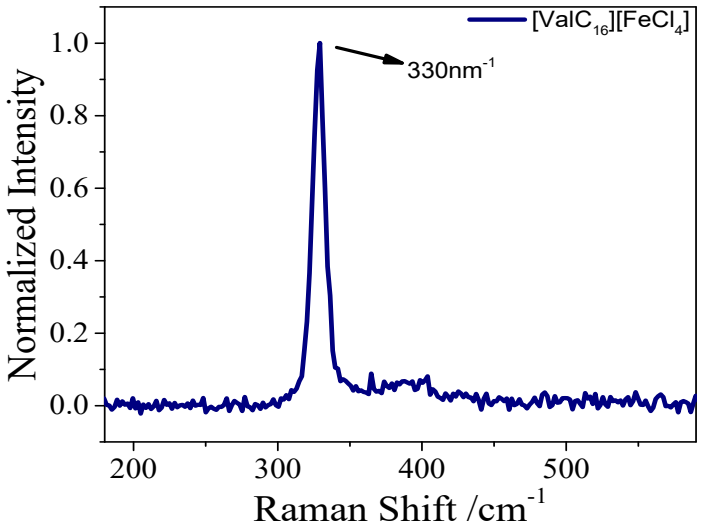


**Fig. S4.** Raman spectra of $[ValC_{16}][FeCl_4]$

## 5. UV spectra of $[ValC_{16}][FeCl_4]$[1]

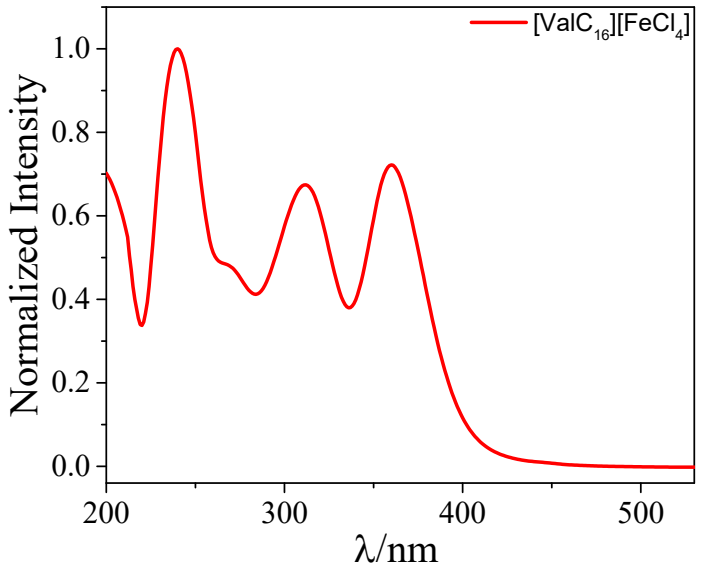


**Fig. S5.** UV spectra of $[ValC_{16}][FeCl_4]$

## 6. EPR spectra of $[ValC_{16}][FeCl_4]$

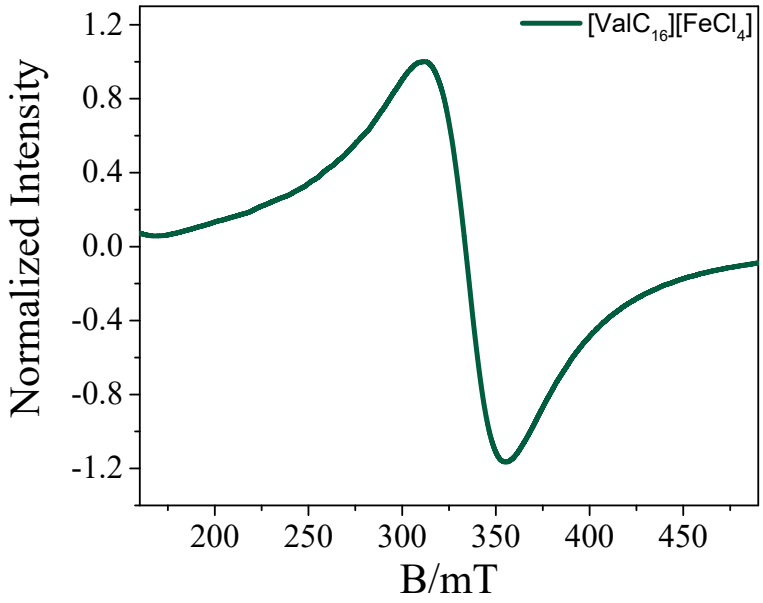


**Fig. S6.** EPR spectra of $[ValC_{16}][FeCl_4]$

## 7. DSC thermogram of $[ValC_{16}][FeCl_4]$ & $[ValC_{16}][Cl]$.

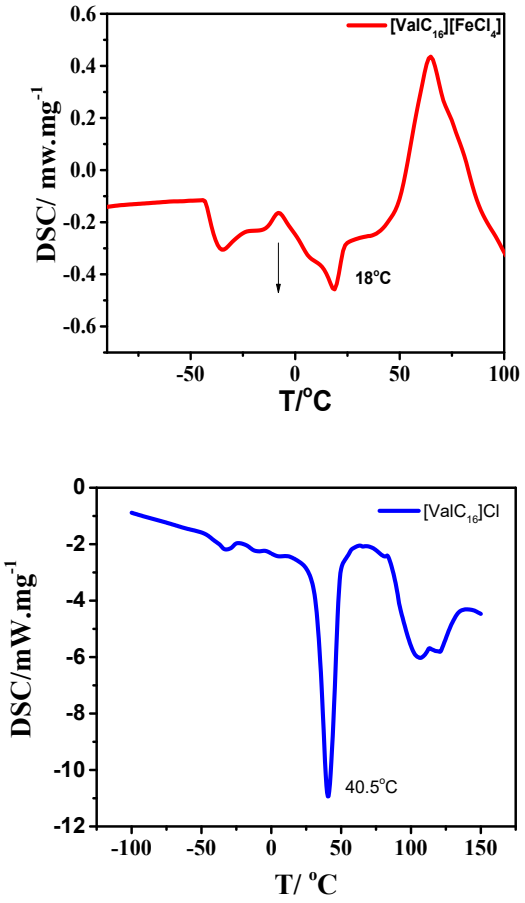


**Fig. S7** DSC thermogram of $[ValC_{16}][FeCl_4]$ & $[ValC_{16}][Cl]$.

## 8. Thermogravimetric analysis and parameters

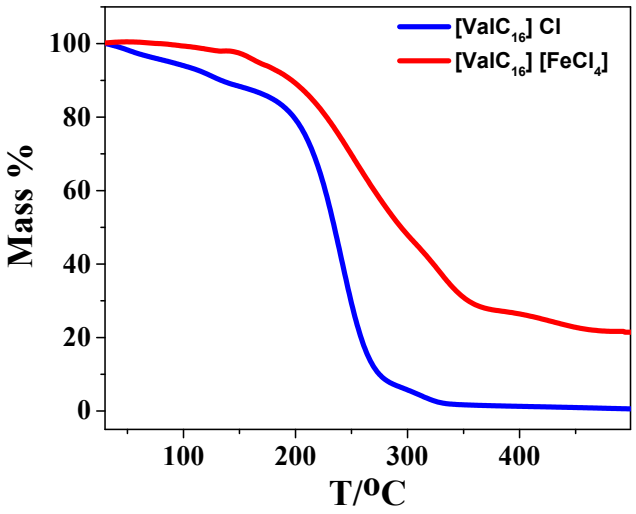


**Fig. S8** TGA analysis of $[ValC_{16}][FeCl_4]$ & $[ValC_{16}][Cl]$.

## 9. Thermal parameters of $[ValC_{16}][FeCl_4]$ & $[ValC_{16}][Cl]$.

**Table S1: $T_d$, $T_{start}$ and $T_{onset}$ of $[ValC_{16}][FeCl_4]$ & $[ValC_{16}]Cl$.**

| SAILs | $T_{start}$(°C) | $T_d$ (°C) | $T_{onset}$(°C) |
|---|---|---|---|
| $[ValC_{16}][Cl]$ | 174 | 242 | 193 |
| $[ValC_{16}][FeCl_4]$ | 180 | 251 | 207 |

## 10. Wavelength vs $I_1/I_3$ graph

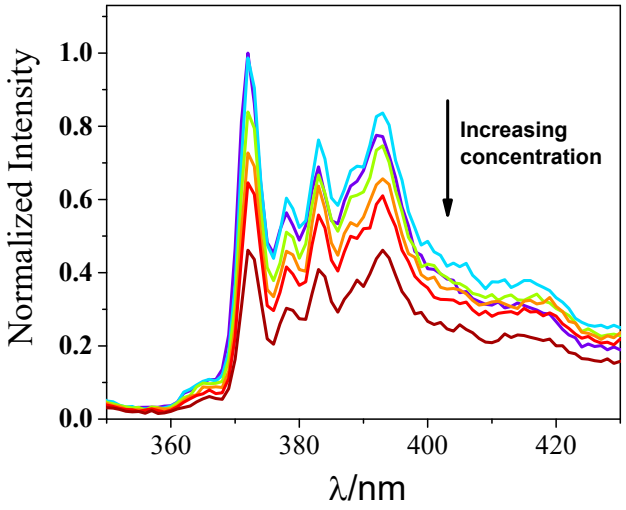


**Fig. S9** Wavelength vs $I_1/I_3$ on increasing concentration of [$ValC_{16}$][$FeCl_4$].

## 11. Concentration dependent morphological transitions in [$ValC_{16}$][$FeCl_4$].

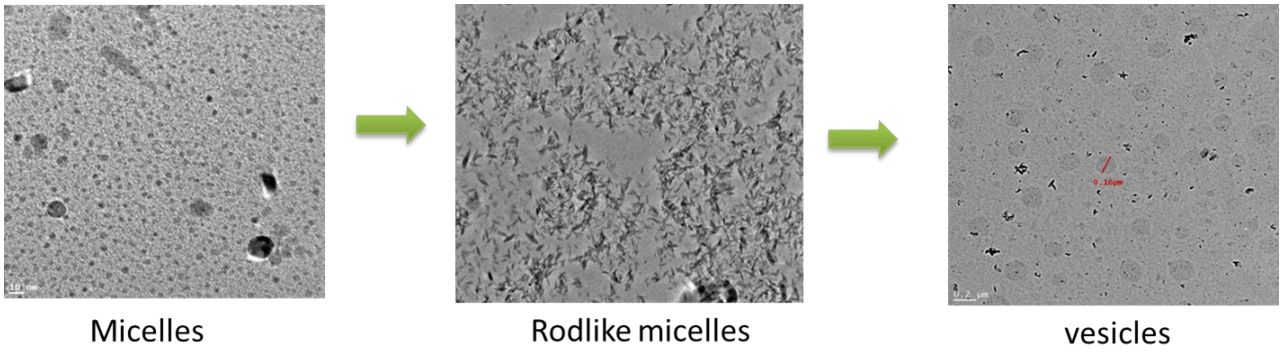


**Fig. S10** Concentration dependent morphological transitions in [$ValC_{16}$][$FeCl_4$].

## 12. DLS plot of micelle formation using $[ValC_{16}][FeCl_4]$

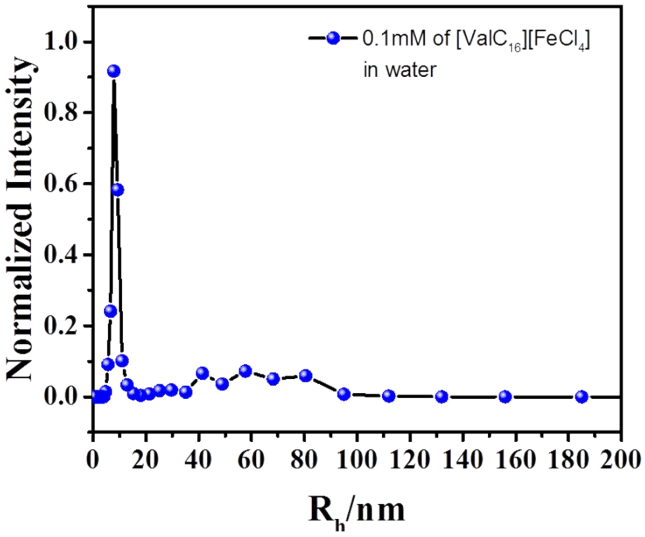


**Fig. S11** DLS plot of micelle using $[ValC_{16}][FeCl_4]$

## 13. Autocorrelation function of $[ValC_{16}][FeCl_4]$.

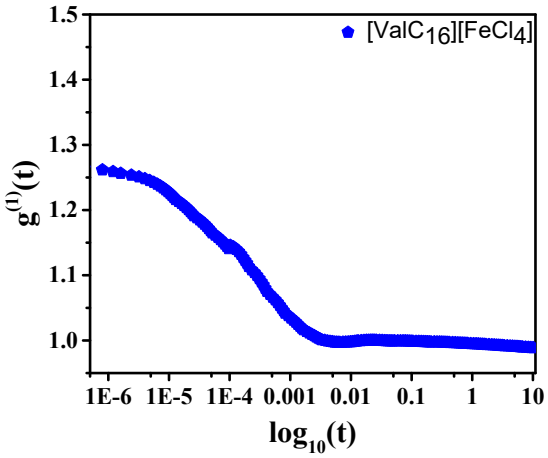


**Fig. S12.** Autocorrelation function of $[ValC_{16}][FeCl_4]$.

## 14. Zeta Potential of Micelles and vesicles of [$ValC_{16}$][$FeCl_4$]

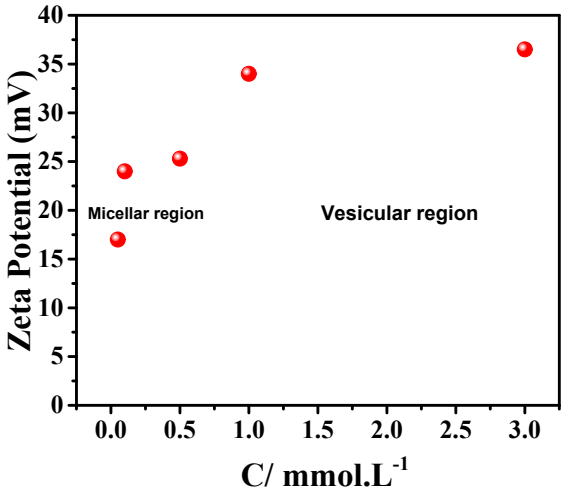


**Fig. S13** Zeta Potential of Micelles and vesicles of [$ValC_{16}$][$FeCl_4$]

## 15. EDX elemental mapping of Gelatin- [$ValC_{16}$][$FeCl_4$] biocomposite gel

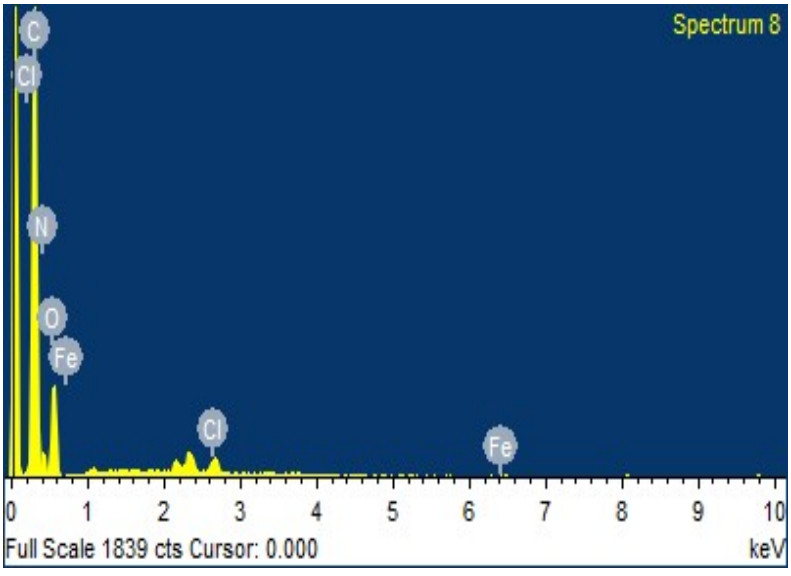

**Fig. S14** EDX elemental mapping of Gelatin-[$ValC_{16}$][$FeCl_4$] biocomposite gel

**16. Stability of gelatin- [$ValC_{16}$][$FeCl_4$] biocomposite gel**

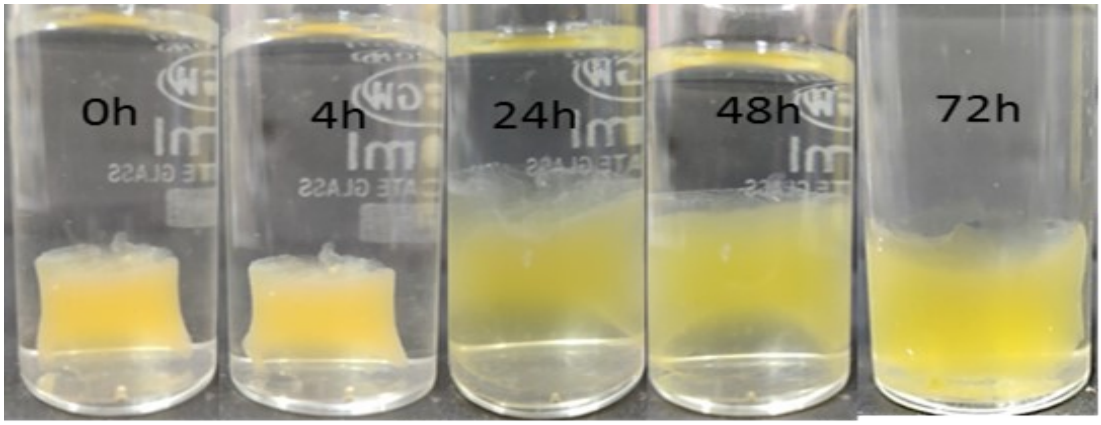


**Fig. S15** Stability of gelatin-[$ValC_{16}$][$FeCl_4$] biocomposite gel.

**17. Swelling behavior of gelatin-[$ValC_{16}$][$FeCl_4$] biocomposite gel**

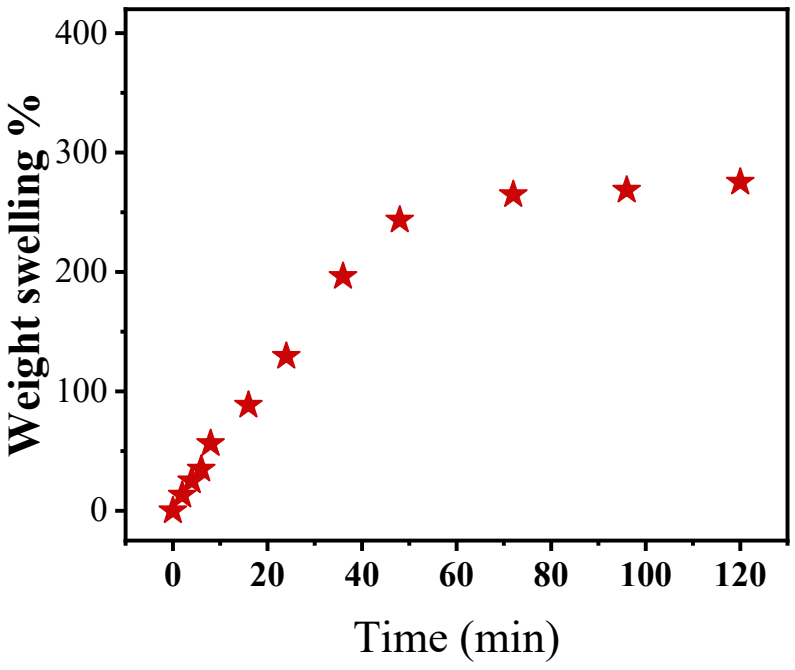


**Fig. S16** Swelling behavior of gelatin-[$ValC_{16}$][$FeCl_4$] biocomposite gel

**18. Comparison of previously reported ornidazole drug loading efficiency in various systems.**

**Table S2** Comparison of previously reported ornidazole drug loading efficiency in various systems.

| S.No | Materials | Loading efficiency of Oridazole(%) | Author | Year |
|---|---|---|---|---|
| 1. | Present work (magnetic biocomposite gel) | 69.3% | - | - |
| 2. | Beta-cyclodextrin polymer microspheres (βCDPM) | 8.86% | Y. Liu et al.[2] | 2020 |
| 3. | PVP electrospun fibers | - | S. Tort et al. [3] | 2018 |
| 4. | Polyethylene glycol-based micron-level particle | 15-20% | S. Tamilvanan et al.[4] | 2019 |
| 5. | Ornidazole-Loaded Graphene Paper | 10-17.3% | W. Quian et al.[5] | 2018 |
| 6. | Biopolymer-dextrin and poly(methyl methacrylate) microgel | 30.54 % | D. Das et al. [6] | 2016 |
| 7. | Biocompatible hydrogel derived from glycogen and poly(N-isopropylacrylamide) | 19-31 % | Priyapratim Patra et al.7 | 2016 |

**19. Comparison of previously reported 5-Fluoro uracil drug loading efficiency in various systems.**

**Table S3** Comparison of previously reported 5-Fluoro uracil drug loading efficiency in various systems.

| S.No | Materials | Loading efficiency of 5-FU (%) | Author | Year |
|---|---|---|---|---|
| 1. | Present work (magnetic biocomposite gel) | 78.3% | - | - |
| 2. | Poly(ϵ-caprolactone) with 6-(chloromethyl)uracil | 42% | S. Zhu et al. [8] | 2020 |
| 3. | Gelatin–rosin gum complex nanoparticle | 50% | S. Joshi [9] | 2020 |
| 4. | polyurethane-based hydrogels | 45-54 % | M. Kamaci et al. [10] | 2020 |
| 5. | PEGylated Ag2S QDs functionalized with Cetuximab (Cet) antibody | 7.34% | F. D. Dumanet al.[11] | 2019 |
| 6. | zinc nanoMOFs functionalized with folate | 24% | B.Yang et al. [12] | 2017 |
| 7. | Self-Assembling Monomeric Nucleoside Molecular Nanoparticle | 53% | H. Zhao et al. [13] | 2015 |

## 20. Kinetics study of drug release pattern using mathematical models

**Table S4:** Kinetics study of release of guest drugs by various mathematical models.

| Guest Molecule | Release condition | *Zero Order | | *First order | | *Higuchi Model | | *KorsMeyar Peppas | | *Hixon Crowell | |
|---|---|---|---|---|---|---|---|---|---|---|---|
| | | $R^2$ | Slope | $R^2$ | Slope | $R^2$ | Slope | $R^2$ | Slope | $R^2$ | Slope |
| Ornidazole | pH 7.4 | 0.83 | 0.75 | 0.89 | 0.006 | 0.93 | 8.3 | 0.98 | 0.62 | 0.87 | 0.018 |
| 5-Fluoro Uracil | pH 7.4 | 0.72 | 0.42 | 0.85 | 0.005 | 0.86 | 6.88 | 0.97 | 0.58 | 0.85 | 0.012 |

## 21. Drug release pattern in different electrolyte solutions

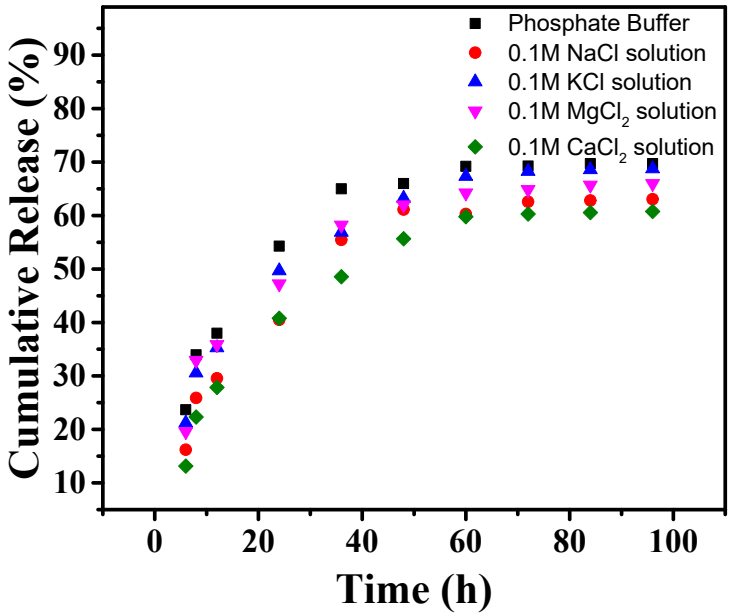


**Fig. S17** Drug release pattern in different electrolyte solution

**Annexure I**

**The Surface parameter equations are as follow:**

1. The Adsorption efficiency( $pC_{20}$ ) and Effectiveness of Surface tension reduction($\Pi_{CAC}$) of surfactant at air-water interface is estimated by using the relation (1)

$$pC_{20} = -\log C_{20}, \qquad \pi_{CMC} = \gamma_{H_2O} - \gamma_{CAC} \text{.....(1)}$$

where, $C_{20}$ is the concentration reduce by 20mNm$^{-1}$ from the surface tension of the solvent (water)[1], $\gamma_{H_2O}$ stands for the surface tension of the pure water and $\gamma_{CMC}$ stands for the surface tension of the solvent medium at CAC.

2. The amount of surfactants adsorbed at the interface is estimated from relative surface excess concentration ($\Gamma_{max}$).The values $\Gamma_{max}$ of at the CMC have been calculated using Gibbs adsorption Eq. 2.

$$\Gamma_{max} = -\frac{1}{nRT}\frac{\partial\gamma}{\partial \ln C} \text{.....(2)}$$

where "$\partial\gamma/\partial \ln C$'' is the slope of $\gamma - \ln C$ plot in the pre *CMC* region and n is Gibbs adsorption coefficient.

3. Minimum area occupied by monomers at the interface was calculated using equation 4.

$$A_{min} = \frac{10^{16}}{\Gamma_{max}.N_A} \text{.....(3)}$$

where $N_A$ is Avogadro number and the Unit of $A_{min}$ is Å$^2$.

4. The β value is obtained from the formula (β =1-α) where the α is the degree of counterion dissociation which is obtained by ratio of the slope post micellar region and the pre micellar region ($S_2/S_1$) then the β value is further used to derive the value of standard free energy of micellization from the equation as follow:

$$\Delta G^o_{mic} = (1+\beta)RT \ln X_{cmc} \text{ ..... (4)}$$

## Annexure-II

### Various mathematical models and their equations

1. Zero order mathematical model:

$$C_o - C_t = K_o t$$

where $C_o$ = intial concentration of the drug at time, t = 0, $C_t$ = amount of drug released at time t, $K_o$ = zero order constant

2. First Order mathematical model:

$$\ln C = \ln C_o - K_1 t$$

where $C_o$ = intial concentration of the drug at time $K_1$ = first order rate constant, C = percent of drug remaining at time

3. Higuchi model:

$$Q = A\sqrt{D(2Co - Cs)Cst}$$

Q=Cumulative amount of drug released at time per unit area, $C_S$ is the drug solubility in the matrix and D is the diffusion coefficient of the drug molecule in the matrix, $C_S$ =drug solubility in the matrix.

4. Korsmeyer- Peppas model

$$M_t/M_\infty = K_{kp}\, t^n$$

Mt = amount of drug released in time t, M∞ = amount of drug released after time ∞, n = diffusional exponent or drug release exponent, and $K_{kp}$ = Korsmeyer release rate constant.

5. Hixson–Crowell model

$$C_0^{1/3} - C_t^{1/3} = K_{HC} t$$

$K_{HC}$= Hixson–Crowell constant

### References

1. Vander Hoogerstraete, T.; Wellens, S.; Verachtert, K.; Binnemans, K., Removal of transition metals from rare earths by solvent extraction with an undiluted phosphonium ionic liquid: separations relevant to rare-earth magnet recycling. *Green Chemistry* **2013,** *15* (4), 919-927.
2. Liu, Y.; Tang, P.; Pu, H.; Qian, H.; Sun, Q.; Zhao, L.; Li, M.; Li, H., Study on the synthesis and drug-loading optimization of beta-cyclodextrin polymer microspheres containing ornidazole. *Journal of Drug Delivery Science and Technology* **2020,** *58*, 101836.
3. Tort, S.; Yıldız, A.; Tuğcu-Demiröz, F.; Akca, G.; Kuzukıran, Ö.; Acartürk, F., Development and characterization of rapid dissolving ornidazole loaded PVP electrospun fibers. *Pharmaceutical Development and Technology* **2019,** *24* (7), 864-873.
4. Tamilvanan, S.; Chanda, P., Ornidazole-loaded polyethylene glycol-based micron-level particles: influence of eutectic liquid on reservoir-type particle formation, drug entrapment efficiency and drug dissolution or release behavior. *Polymer Bulletin* **2019,** *76* (9), 4389-4398.
5. Qian, W.; Wang, Z.; He, D.; Huang, X.; Su, J., Ornidazole-loaded graphene paper for combined antibacterial materials. *Journal of Saudi Chemical Society* **2018,** *22* (5), 581-587.
6. Das, D.; Rameshbabu, A. P.; Patra, P.; Ghosh, P.; Dhara, S.; Pal, S., Biocompatible amphiphilic microgel derived from dextrin and poly(methyl methacrylate) for dual drugs carrier. *Polymer* **2016,** *107*, 282-291.
7. Patra, P.; Rameshbabu, A. P.; Das, D.; Dhara, S.; Panda, A. B.; Pal, S., Stimuli-responsive, biocompatible hydrogel derived from glycogen and poly(N-isopropylacrylamide) for colon targeted delivery of ornidazole and 5-amino salicylic acid. *Polymer Chemistry* **2016,** *7* (34), 5426-5435.
8. Zhu, S.; Wen, L.; Xiao, Y.; Lang, M., Poly(ε-caprolactone) with pH and UCST responsiveness as a 5-fluorouracil carrier. *Polymer Chemistry* **2020,** *11* (32), 5173-5180.
9. Joshi, S.; Singh, V., Gelatin–rosin gum complex nanoparticles: preparation, characterization and colon targeted delivery of 5-fluorouracil. *Chemical Papers* **2020,** *74* (12), 4241-4252.
10. Kamaci, M., Polyurethane-based hydrogels for controlled drug delivery applications. *European Polymer Journal* **2020,** *123*, 109444.
11. Duman, F. D.; Akkoc, Y.; Demirci, G.; Bavili, N.; Kiraz, A.; Gozuacik, D.; Acar, H. Y., Bypassing pro-survival and resistance mechanisms of autophagy in EGFR-positive lung cancer cells by targeted delivery of 5FU using theranostic Ag2S quantum dots. *Journal of Materials Chemistry B* **2019,** *7* (46), 7363-7376.
12. Yang, B.; Shen, M.; Liu, J.; Ren, F., Post-Synthetic Modification Nanoscale Metal-Organic Frameworks for Targeted Drug Delivery in Cancer Cells. *Pharmaceutical Research* **2017,** *34* (11), 2440-2450.
13. Zhao, H.; Feng, H.; Liu, D.; Liu, J.; Ji, N.; Chen, F.; Luo, X.; Zhou, Y.; Dan, H.; Zeng, X.; Li, J.; Sun, C.; Meng, J.; Ju, X.; Zhou, M.; Yang, H.; Li, L.; Liang, X.; Chu, L.; Jiang, L.; He, Y.; Chen, Q., Self-Assembling Monomeric Nucleoside Molecular Nanoparticles Loaded with 5-FU Enhancing Therapeutic Efficacy against Oral Cancer. *ACS Nano* **2015,** *9* (10), 9638-9651.